Runx3 drives a CD8$^+$ T cell tissue residency program that is absent in CD4$^+$ T cells

Raíssa Fonseca[1,10], Thomas N. Burn[1,10], Luke C. Gandolfo[1,2,3], Sapna Devi[1], Simone L. Park[1], Andreas Obers[1], Maximilien Evrard[1], Susan N. Christo[1], Frank A. Buquicchio[6,7], Caleb A. Lareau[6,7], Keely McDonald[1], Sarah K. Sandford[1], Natasha M. Zamudio[1], Nagela G. Zanluqui[1,4], Ali Zaid[5], Terence P. Speed[2,3], Ansuman T. Satpathy[6,7,8,9], Scott N. Mueller[1], Francis R. Carbone[1,11] and Laura K. Mackay[1,11,*]

[1]Department of Microbiology and Immunology, The University of Melbourne at The Peter Doherty Institute for Infection and Immunity, Melbourne, VIC, Australia.
[2]School of Mathematics and Statistics, The University of Melbourne, Melbourne, VIC, Australia.
[3]Walter and Eliza Hall Institute for Medical Research, Parkville, VIC, Australia.
[4]Department of Immunology, Institute of Biomedical Sciences, University of São Paulo, São Paulo, SP, Brazil.
[5]Menzies Health Institute Queensland, Griffith University, Gold Coast Campus, Southport, QLD, Australia.
[6]Department of Pathology, Stanford University, Stanford, CA, USA.
[7]Program in Immunology, Stanford University, Stanford, CA, USA.
[8]Parker Institute for Cancer Immunotherapy, Stanford University, Stanford, CA, USA.
[9]Gladstone-UCSF Institute of Genomic Immunology, San Francisco, CA, USA.
[10] These authors contributed equally to this work.
[11] These authors jointly directed this work.
*Correspondence: lkmackay@unimelb.edu.au (L.K.M.)

Abstract

Tissue-resident memory T cells (T_{RM} cells) provide rapid and superior control of localised infections. While the transcription factor Runx3 is a critical regulator of $CD8^+$ T cell tissue residency, its expression is repressed in $CD4^+$ T cells. Here, we show that as a direct consequence of this Runx3-deficiency, $CD4^+$ T_{RM} cells lack the TGFβ-responsive transcriptional network that underpins the tissue residency of epithelial $CD8^+$ T_{RM} cells. While $CD4^+$ T_{RM} cell formation requires Runx1, this along with the modest expression of Runx3 in $CD4^+$ T_{RM} cells was insufficient to engage the TGFβ-driven residency program. Ectopic expression of Runx3 in $CD4^+$ T cells induced a TGFβ-transcriptional network to promote prolonged survival, decreased tissue egress, a microanatomical redistribution towards epithelial layers and enhanced effector functionality. Thus, our results reveal distinct programming of tissue residency in $CD8^+$ and $CD4^+$ T_{RM} cell subsets that is attributable to divergent Runx3 activity.

Introduction

Following pathogen clearance, memory T cells can persist in a variety of locations throughout the body. Some of these memory cells form a non-migratory tissue-resident memory T cell (T_{RM} cell) population that surveys the local microenvironment and provides critical control of *de novo* infections[1, 2]. The events driving $CD8^+$ T_{RM} cell formation have been extensively studied, revealing a range of intrinsic and extrinsic factors involved in $CD8^+$ T_{RM} cell development, and the detailed transcriptional pathways that control these events[3, 4, 5, 6]. Local environmental mediators are indispensable for $CD8^+$ T_{RM} cell formation, with the cytokine TGFβ acting as a pivotal extrinsic catalyst for full $CD103^+$ T_{RM} cell maturation in tissues such as the skin and intestine[7, 8]. TGFβ receptor engagement results in a range of phenotypic and functional changes that are orchestrated by intrinsic transcriptional regulators[9]. Embedded at the core of this T_{RM} cell transcriptional network are transcription factors such as Klf2, Hobit and Runx3, which initiate the residency program in $CD8^+$ T cells by shutting down tissue egress and upregulating a range of molecules required for long-term persistence and survival[10, 11, 12].

The expression of the canonical T_{RM} cell marker CD103, used to identify epithelial $CD8^+$ T_{RM} cells, is less uniform in $CD4^+$ T cells[13], complicating the identification of *bona fide* $CD4^+$ T_{RM} cells. Nonetheless, there is compelling evidence for $CD4^+$ T_{RM} cell formation in a variety of settings[14, 15, 16, 17] and there are many commonalities between $CD4^+$ and $CD8^+$ T_{RM} cell populations, such as the expression of CD69 and CXCR6, and downregulation of the tissue egress molecules S1PR1 and CCR7[13, 18]. However, unlike $CD8^+$ T_{RM} cell development, $CD4^+$ T cell residency depends on the presence of a combination of B cells, $CD8^+$ T cells and mononuclear phagocyte clusters, with the possibility of antigen co-involvement[16, 19, 20]. In addition, differences in the location of $CD4^+$ and $CD8^+$ T cells in peripheral tissues have been documented, with the former occupying underlying regions such as the dermis in the skin and the lamina propria in the small intestine[13, 19, 21], while the latter is apparent in the epithelial regions directly exposed to external environments and pathogens[21, 22, 23]. This difference in localisation correlates with differing immune surveillance by these T cell subsets in skin, where $CD4^+$ T cells display dynamic movement, while $CD8^+$ T_{RM} cells monitor more restricted areas[21].

The transcription factor Runx3 is a critical regulator of $CD8^+$ T_{RM} cell programming[12]. Runx3 and its paralog Runx1 are both involved in the early stages of T cell lineage commitment and have overlapping genomic binding sites[24], but their expression is subsequently segregated during T cell maturation, with Runx3 driving $CD8^+$ T cell lineage determination and functionality[25]. In conventional $CD4^+$ T cells, Runx3 is downregulated by ThPOK, which drives $CD4^+$ T cell development[26] and $CD4^+$ memory T cell formation[27]. While Runx3 is normally repressed in naïve $CD4^+$ T cells, its upregulation is required for T_H1 lineage specification[28]. Conversely, Runx1 is highly expressed in naïve $CD4^+$ T cells and is similarly involved in T_H1 polarisation[29]. Whether these transcription factors cooperate beyond this early polarisation stage in $CD4^+$ T cell activation, especially during memory cell embodiment, during which Runx3 plays a critical role in the establishment of $CD8^+$ T_{RM} cells in peripheral tissues is unclear[12].

Here we investigated whether Runx3 controlled tissue residency in $CD4^+$ T_{RM} cells and whether the same regulatory mechanism as $CD8^+$ T_{RM} cells were employed, either via residual Runx3 expression or by the action of alternative regulators. We show that Runx3 enforced tissue residency in $CD8^+$ T cells through a TGFβ-dependent transcriptional mechanism that was absent in $CD4^+$ T_{RM} cells. While $CD4^+$ tissue residency relied on the expression of Runx1, this did not compensate for the lack of Runx3, leading to reduced $CD4^+$ T_{RM} cell maintenance in epithelial layers and limited effector capacity. Altogether, this work indicated that $CD4^+$ and $CD8^+$ T_{RM} cells were not equivalent in terms of tissue residency and that this discordance was a direct consequence of the divergent expression of Runx3.

Results

Runx1 and Runx3 differentially program CD4$^+$ and CD8$^+$ T_{RM} cells

CD4$^+$ and CD8$^+$ T_{RM} cells are phenotypically and transcriptionally distinct, correlating with their divergent localisation in barrier tissues[13, 19, 21]. To explore whether this microanatomical discordance was underpinned by transcriptional differences between CD4$^+$ and CD8$^+$ T_{RM} cells, we infected the skin of C57BL/6 mice with herpes simplex virus (HSV), a model where virus-specific CD8$^+$ (gBT-I) and CD4$^+$ (gDT-II) transgenic T cells segregate into epidermal and dermal layers respectively, by 30 days post-infection (**Fig. 1a, b**). Similarly, following the transfer of lymphocytic choriomeningitis virus (LCMV)-specific CD8$^+$ (P14) and CD4$^+$ (SMARTA) transgenic T cells into C57BL/6 mice infected with LCMV, CD8$^+$ T_{RM} cells occupied the small intestine intraepithelial lymphocyte (SI-IEL) compartment while CD4$^+$ T_{RM} cells were largely restricted to the lamina propria (SI-LP) 30 days post-infection (**Extended Data Fig. 1a, b**). CD8$^+$ T_{RM} cells in the SI-IEL and skin formed homogenous CD69$^+$CD103$^+$ populations, while CD4$^+$ T cells in the skin or SI-IEL exhibited low expression of CD103 (**Extended Data Fig. 1c-f**).

Runx3 has a critical role in driving CD8$^+$ T_{RM} cell development, promoting CD103 expression and epithelial localisation[12]. Since Runx3 expression is lower in CD4$^+$ T cells in comparison to CD8$^+$ T cells (**Fig. 1c, Extended Data Fig. 1g**), we investigated whether Runx family members differentially regulated CD8$^+$ and CD4$^+$ T_{RM} cell development. First, we profiled the expression of Runx1 and Runx3 in tissue-resident CD69$^+$CD4$^+$ (CD4$^+$ T_{RM}) SMARTA cells from the SI-LP, CD69$^+$CD103$^+$CD8$^+$ (CD8$^+$ T_{RM}) P14 cells from the SI-IEL, and endogenous naïve (CD44$^-$ CD62L$^+$) CD4$^+$ and CD8$^+$ T cells from the spleen, 30 days post-LCMV infection. Runx1 expression was highest in naïve CD4$^+$ T cells and then SI-LP CD4$^+$ T_{RM} cells, while Runx3 expression was highest in SI-IEL CD8$^+$ T_{RM} cells (**Fig. 1d, e**), consistent with skin CD8$^+$ T_{RM} cells (**Fig. 1c**). Runx3 expression was low in naïve CD4$^+$ T cells, increased upon T cell activation[27, 28] (**Extended Data Fig. 1h, i**), and remained elevated in CD69$^+$CD4$^+$ T_{RM} cells from the skin or SI-LP compared to splenic naïve (CD44$^-$CD62L$^+$) or circulating memory (CD44$^+$) CD4$^+$ T cells (CD4$^+$ T_{CIRC}) (**Fig. 1c-e**). However, Runx3 expression in CD4$^+$ T cells remained lower than in CD69$^+$CD103$^+$CD8$^+$ T_{RM} cells in the skin and SI-IEL more than 30 days post-infection (**Fig. 1c-e**). While Runx3 expression was positively correlated with CD103 expression, Runx1 was inversely, or not correlated with CD103 (**Fig. 1f, Extended Data Fig.**

1j). This suggested distinct roles for Runx1 and Runx3 in programming $CD103^+$ T_{RM} cells and that high expression of Runx3 is required for $CD103^+$ T_{RM} cell programming.

Next, we used CRISPR-Cas9 to ablate either Runx1 (sgRunx1), Runx3 (sgRunx3), or CD19 (Ctrl) in $CD8^+$ gBT-I cells, or $CD4^+$ gDT-II cells (**Extended Data Fig. 1k, l**) to determine the functional roles of these transcription factors in driving T_{RM} cell formation. First, *in vitro* activated $CD8^+$ sgRunx1 or $CD8^+$ sgRunx3 cells were co-transferred with $CD8^+$ Ctrl cells intradermally (i.d.) into the skin of naïve C57BL/6 mice. At least 20 days post-transfer, we observed a 1.7-fold decrease in $CD69^+CD103^+CD8^+$ sgRunx1 cells, and a 96-fold decrease in $CD69^+CD103^+CD8^+$ sgRunx3 cells compared to Ctrl cells in the skin (**Fig. 1g, h**). CD103 expression was reduced by more than 60% on $CD69^+CD8^+$ sgRunx3 cells, while CD103 expression on $CD69^+CD8^+$ sgRunx1 cells was unchanged (**Fig. 1i**). Next, *in vitro* activated $CD4^+$ sgRunx1 cells or $CD4^+$ sgRunx3 cells were co-transferred with $CD4^+$ Ctrl cells i.d. into the skin of naïve C57BL/6 mice. At least 20 days post-transfer we observed a 2-fold decrease in $CD69^+CD4^+$ sgRunx1 cells compared to Ctrl cells in the skin, while $CD69^+CD4^+$ sgRunx3 cells were unaffected (**Fig. 1j, k**). Expression of CD103 was unchanged on $CD69^+CD4^+$ sgRunx1 or sgRunx3 cells (**Fig. 1l**). We similarly ablated Runx1 expression in naïve $CD4^+$ SMARTA cells that were co-transferred with control (Ctrl) cells intravenously (i.v.) into C57BL/6 mice that were then infected with LCMV. At 30 days post-infection, $CD4^+$ sgRunx1 cells were reduced by 5-fold in the spleen, but $CD69^+CD4^+$ sgRunx1 cells in the SI-IEL were reduced by 13-fold compared to Ctrl cells (**Extended Data Fig. 1m**). Together, these data indicate that $CD4^+$ T cells required Runx1 for T_{RM} cell development, however, neither Runx1 nor intermediate expression of Runx3 was sufficient for the acquisition of the epithelial $CD103^+$ T_{RM} cell phenotype intrinsic to the $CD8^+$ T cell population.

Runx3 enables epithelial $CD4^+$ T cell residency

Ectopic expression of Runx3 augments $CD103^+CD8^+$ epithelial T_{RM} cell development[12]. We sought to determine whether ectopic expression of Runx3 in $CD4^+$ T cells permits these cells to adopt a $CD8^+$ T_{RM} cell-like phenotype. Runx3 was ectopically expressed in $CD8^+$ gBT-I cells (CD8-Runx3) or $CD4^+$ gDT-II cells (CD4-Runx3) using a Runx3-encoding retrovirus[12], and control (CD8-Ctrl or CD4-Ctrl) cells transduced with GFP-encoding retrovirus. CD8-Ctrl and CD8-Runx3 cells were co-transferred into HSV infected mice. At 14 days post-infection, $CD127^+$ CD8-Runx3 cells in the spleen were unchanged, while $CD69^+$ CD8-Runx3 cells in the

skin epithelium were increased 1.5-fold alongside elevated CD103 expression, compared to CD8-Ctrl cells (**Fig. 2a-c**). Similar observations were found in the context of LCMV infection, where CD8-Ctrl and CD8-Runx3 P14 cells were co-transferred i.v. into LCMV infected mice and $CD69^+CD103^+$ CD8-Runx3 cells were increased 5.6-fold in the SI-IEL and 3.5-fold in the skin, when compared to CD8-Ctrl cells at 14 days post-infection (**Extended Data Fig. 2a, b**). Next, CD4-Runx3 and CD4-Ctrl gDT-II cells were co-transferred i.v. into HSV-infected mice. At day 14 post-infection, CD4-Runx3 cells were unaltered in the spleen, but $CD69^+$ CD4-Runx3 cells in the skin were increased by 2.3-fold compared to CD4-Ctrl cells (**Fig. 2d, e, Extended Data Fig. 3a**). CD4-Runx3 cells accounted for 74% of the transferred cells in the skin epithelium (**Fig. 2f, Extended Data Fig. 3b**) and CD103 and CD49a expression was increased by 43% and 36% respectively in CD4-Runx3 cells compared to CD4-Ctrl cells (**Fig. 2g, h, Extended Data Fig. 3c**). Similarly, CD4-Ctrl and CD4-Runx3 SMARTA cells were co-transferred i.v. into LCMV-infected mice treated on the skin with DNFB and at 14 days post-infection, CD4-Runx3 cells were increased in both the SI-IEL and skin (4.1 and 11-fold, respectively) compared to CD4-Ctrl cells (**Extended Data Fig. 3d-f**).

Runx3 can drive conversion of $CD4^+$ T cells into $CD8\alpha\alpha^+$ T cells in the SI-IEL[30] (**Extended Data Fig. 3g, h**). Ectopic expression of Runx3 did not induce the expression of CD8α, nor abrogate expression of ThPOK in CD4-Runx3 cells (**Fig. 2i**). While expression of Runx3 was higher in CD4-Runx3 cells than $CD8^+$ T cells *in vitro* (**Fig. 2i**), it was equivalent to endogenous $CD8^+$ T cells *in vivo* (**Fig. 2j, Extended Figure 3i**). Altogether, these findings indicated that increased expression of Runx3 in $CD4^+$ T cells was necessary and sufficient to permit the accumulation of $CD4^+$ T_{RM} cells in epithelial locations, without conversion to the $CD8\alpha\alpha^+$ lineage.

Runx3 induces a CD8-like T_{RM} cell program in $CD4^+$ T cells

Next we employed RNA sequencing (RNA-seq) to define the complete suite of transcriptional changes associated with ectopic expression of Runx3 in $CD4^+$ T cells. For this, HSV-specific CD4-Runx3, CD4-Ctrl and CD8-Ctrl cells were co-transferred i.v. into HSV infected mice, and cells isolated from the skin at day 14 post-infection. Principal component analysis (PCA) showed that while CD4-Runx3 cells differed transcriptionally from CD4-Ctrl and CD8-Ctrl cells (**Fig. 3a**), 347 differentially expressed genes were shared between CD4-Runx3 and CD8-

Ctrl cells compared to CD4-Ctrl cells (**Fig. 3b**). We utilised gene set enrichment analysis (GSEA) to compare genes that were up- or down-regulated in CD8-Ctrl cells, to those altered by the enforced expression of Runx3 in $CD4^+$ T cells. This data demonstrated that CD4-Runx3 cells acquired a striking transcriptional resemblance to CD8-Ctrl cells (**Fig. 3c, d**). *Cd101, Cdh1, Xcl1, Rgs2, Cmah,* and *Litaf,* were upregulated and *Il7r, Ly6c and S1pr1* were downregulated in CD4-Runx3 cells (**Fig. 3d, e**), changes consistent with adoption of the $CD8^+$ T_{RM} cell core transcriptional signature[31]. Comparison of the transcriptome of CD4-Runx3 cells with a published $CD8^+$ T_{RM} cell signature derived from skin $CD8^+$ T_{RM} cells and spleen T_{CIRC} cells[11] indicated CD4-Runx3 cells were strongly enriched for the $CD8^+$ T_{RM} cell signature (**Fig. 3f**). The transcriptomes of CD4-Runx3 and CD8-Ctrl cells correlated with that of *bona fide* $CD8^+$ skin T_{RM} cells[11] (**Fig. 3f, g, Extended Data Fig. 4a-d**). Overall, these data indicated that expression of Runx3 in $CD4^+$ T cells specifically drove the transcription of genes associated with tissue residency.

Runx3 remodels chromatin to enable a TGFβ-driven T_{RM} cell program

Given the dual requirement of Runx3 and TGFβ for epithelial $CD8^+$ T_{RM} cell development[7, 9, 32], we hypothesised that high expression of Runx3 may be necessary to enhance chromatin accessibility at TGFβ-regulated, $CD8^+$ T_{RM} cell-specific genes. To test this, we examined the epigenetic landscape of CD4-Ctrl, CD4-Runx3, CD8-Ctrl and CD8-Runx3 cells treated *in vitro* with TGFβ by ATAC-seq. CD4-Runx3 cells had an epigenetic landscape similar to CD8-Ctrl cells, irrespective of TGFβ treatment (**Fig. 4a**). Runx3 motif accessibility was enhanced in CD4-Runx3 cells to a level equivalent to CD8-Ctrl cells, and this was not influenced by TGFβ treatment (**Fig. 4b**). CD8-Ctrl and CD4-Runx3 cells had increased accessibility at TGFβ-dependent genes, compared to CD4-Ctrl cells, indicating that Runx3 specifically enhanced accessibility at TGFβ-regulated regions (**Fig. 4c**). Accessibility at TGFβ-regulated regions was not altered by treatment with TGFβ in CD4-Ctrl, CD4-Runx3, or CD8-Ctrl cells (**Extended Data Fig. 5a, b**). Further, genome track analyses showed increased accessibility at genes associated with $CD8^+$ tissue residency, including *Itgae, Cd244,* and *Pdcd1,* and reduced accessibility at $CD8^+$ T_{CIRC}-associated genes, such as *Ly6c* and *S1pr1* in CD4-Runx3 cells (TGFβ-untreated) (**Fig. 4d, Extended Data Fig. 5c**), consistent with a model in which high expression of Runx3 is necessary for allowing accessibility at TGFβ-regulated, $CD8^+$ T_{RM} cell-associated genes.

Next, we interrogated whether Runx3-induced epigenetic changes were accompanied by TGFβ-driven transcriptional changes. The transcriptome of CD4-Runx3 cells from the skin (**Fig. 3**) was compared to the TGFβ-driven transcriptional signature in $CD8^+$ skin T_{RM} cells[9] (derived from wild-type vs TGFβ-receptor deficient (*Tgfbr2*$^{-/-}$) $CD8^+$ skin T_{RM} cells). GSEA analysis showed that the top 100 TGFβ up- and down-regulated genes were strongly enriched in CD4-Runx3 compared to CD4-Ctrl cells (**Fig. 5a, b**). Transcriptional changes induced by Runx3 in $CD4^+$ T cells were significantly correlated with wide-scale changes induced by TGFβ in $CD8^+$ skin T_{RM} cells [9] (**Fig. 5c, Extended Data Fig. 6a-c**). Overlaying the TGFβ signature on the transcriptional profiles of CD4-Runx3 vs CD4-Ctrl cells, or skin $CD8^+$ T_{RM} vs splenic $CD8^+$ T_{CIRC} cells, and stratifying the genes that were up- or downregulated by TGFβ, indicated a compelling association between Runx3-induced gene expression and TGFβ-driven T_{RM} cell maturation (**Fig. 5c, Extended Data Fig. 6d**).

Together these data suggested that expression of genes required for skin $CD8^+$ T_{RM} cell development required both Runx3 expression and TGFβ-signalling. We validated this co-operative requirement by examining protein-level expression of a selection of TGFβ-dependent genes on wild-type $CD8^+$, *Tgfbr2*$^{-/-}$ $CD8^+$, CD4-Ctrl, and CD4-Runx3 cells treated with TGFβ for 48 hours *in vitro*. TGFβ upregulated CD103, CD244, PD-1, and CD49a, and downregulated Ly6C on wild-type $CD8^+$ and CD4-Runx3 cells, but not *Tgfbr2*$^{-/-}$ $CD8^+$ and CD4-Ctrl cells (**Fig. 5d-h**). Combined, these results indicated that high expression of Runx3 was required to enforce chromatin accessibility at a suite of TGFβ-responsive genes necessary for epithelial $CD8^+$ T_{RM} development, and that the inherent inability of $CD4^+$ T cells to adopt this specific T_{RM} cell fate could be overcome upon sufficient expression of Runx3.

Runx3 requires TGFβ to drive tissue residency *in vivo*

Our results demonstrated that Runx3 drove epigenetic remodelling, prior to TGFβ-induced transcriptional rewiring within CD4-Runx3 cells, suggesting that Runx3-driven enhancement of $CD4^+$ T_{RM} cell development may depend on TGFβ-signalling. To test whether TGFβ-driven Runx3-dependent transcription alterations manifest as differences in skin T_{RM} cell development, wild-type and *Tgfbr2*$^{-/-}$ $CD4^+$ and $CD8^+$ T cells were activated *in vitro* and co-transferred i.d. into the skin of naïve C57BL/6 mice. At 30 days post-transfer, *Tgfbr2*$^{-/-}$

CD69^{+}CD4^{+} cells in the skin were reduced 2.4-fold, while *Tgfbr2*$^{-/-}$ CD69^{+}CD8^{+} cells were reduced 16-fold compared to wild-type cells, thus indicating CD8^{+} skin T_{RM} cells were more dependent on TGFβ-signalling (**Fig 6a**). CD103 expression was 8-fold lower in skin *Tgfbr2*$^{-/-}$ CD8^{+} T cells compared to wild-type CD8^{+} T cells, while CD103 remained unchanged on *Tgfbr2*$^{-/-}$ CD4^{+} cells (**Fig. 6b, c**). Next, wild-type and *Tgfbr2*$^{-/-}$ CD4^{+} T cells were transduced with control (CD4-Ctrl) or Runx3 (CD4-Runx3) retroviruses and transferred i.d. into the skin of naïve C57BL/6 mice. At 14 days post-transfer, wild-type CD4-Runx3 cells from the skin were increased by 2-fold, and CD103 expression was increased 3.5-fold compared to wild-type CD4-Ctrl cells. Runx3 overexpression had no impact on cell numbers, or CD103 expression in *Tgfbr2*$^{-/-}$ cells (**Fig. 6d, e**). Therefore, CD4^{+} T cells require TGFβ-signalling to allow the Runx3-induced enhancement of CD4^{+} skin T_{RM} cell formation.

Runx3 enforces CD8-like immunosurveillance in CD4^{+} T_{RM} cells

CD8^{+} epidermal skin T_{RM} cells are dendritic in morphology and non-migratory, while CD4^{+} T cells are motile and located in the dermis[19, 21] (**Fig. 7a**). We questioned whether CD4-Runx3 cells would adopt the intrinsic morphology and migration properties of CD8^{+} T_{RM} cells. CD4^{+} ubiTomato- and GFP-expressing T cells were transduced with control (ubiTomato-CD4-Ctrl) or Runx3 (GFP-CD4-Runx3) retrovirus respectively, transferred i.d. into the skin of naïve C57BL/6 mice, and two-photon microscopy was used to visualise migration properties *in vivo* at day 14 post-transfer. While ubiTomato-CD4-Ctrl cells were predominantly in the dermis and were spherical in shape, GFP-CD4-Runx3 T cells located in the epidermis, had reduced sphericity (**Fig. 7b-d**) and displayed a dendritic morphology similar to CD8^{+} T cells[21] (**Fig. 7a, b**). GFP-CD4-Runx3 cells were less motile than ubiTomato-CD4-Ctrl cells covering a smaller distance, reduced 2-dimensional displacement, at a decreased overall velocity (**Fig. 7e-h, Extended Data Video 1**). Consistently, explanted skin that was seeded similarly with CD4-Ctrl and CD4-Runx3 cells was cultured overnight and CD4-Runx3 cells were retained within the skin tissue to a greater degree than CD4-Ctrl cells (**Fig. 7i, j**), indicating Runx3 overexpression also induced a reduction in tissue egress.

Finally, to assess whether Runx3 had an impact on CD4^{+} T_{RM} cell functionality, we stimulated CD4-Ctrl and CD4-Runx3 gDT-II cells *in vitro* with PMA/ionomycin and observed that CD4-Runx3 cells co-produced more IFN-γ and TNFα compared to CD4-Ctrl cells (**Fig. 7k,**

Extended Data Fig. 7a). CD4-Ctrl and CD4-Runx3 gDT-II cells were then transferred i.d. into the skin of naïve *Rag1*$^{-/-}$ or C57BL/6 mice, which were then infected with HSV 14 days later. At day 6 post-infection, HSV viral titres were 10-fold lower in *Rag1*$^{-/-}$ mice receiving CD4-Runx3 cells, than mice receiving CD4-Ctrl cells (**Fig. 7l**), and C57BL/6 mice receiving CD4-Runx3 cells had HSV viral titres 5-fold lower than mice receiving CD4-Ctrl cells (**Extended Data Fig. 7b**). Further, C57BL/6 mice receiving CD4-Runx3 cells displayed enhanced recruitment of inflammatory monocytes ($CD3^{-}Ly6G^{-}IA/IE^{-}Ly6C^{+}CD64^{+}CD11b^{+}$), and NK cells ($IA/IE^{-}NKp46^{+}NK1.1^{+}$) at day 3 post HSV infection compared to mice receiving CD4-Ctrl cells (**Extended Data Fig. 7c**), consistent with previously described 'sense and alarm' mechanisms of $CD8^{+}$ T_{RM} cell-mediated protection[20, 34, 35]. Overall, these data showed that transcriptional changes induced by Runx3 translated to a range of altered behavioural and functional characteristics that combined, resulted in enhanced tissue residency and superior peripheral immune protection.

Discussion

One of the most striking difference between $CD4^{+}$ and $CD8^{+}$ T_{RM} cells is the reduced expression of Runx3 in $CD4^{+}$ T cells. While Runx3 expression was not required for skin $CD4^{+}$ T_{RM} cell development, the absence of Runx1, which shares Runx3 DNA-binding motifs, impaired $CD4^{+}$ T_{RM} cell development. Nonetheless, in $CD4^{+}$ T cells, neither Runx1 nor Runx3 were sufficient to enforce the TGFβ-dependent residency program that is required by $CD8^{+}$ T_{RM} cells. High levels of ectopic Runx3 drove alterations to the chromatin landscape in $CD4^{+}$ T cells that permitted the expression of TGFβ-dependent $CD8^{+}$ T_{RM} cell genes, and induced $CD4^{+}$ T_{RM} cells to adopt an epithelial-biased T_{RM} cell program that bolstered protection against HSV infection in the skin. These observations argued that $CD4^{+}$ T_{RM} cells do not acquire the transcriptional programming that characterises $CD8^{+}$ T_{RM} cell tissue residency due to insufficient Runx3 expression.

In contrast to $CD8^{+}$ T cells, TGFβ signalling in $CD4^{+}$ T cells intrinsically drives the formation of regulatory T cells (T_{reg} cell) and T_H17 polarisation[37, 38]. Runx3 can circumvent these transformations, and together with TGFβ-signalling direct the differentiation of towards a non-conventional $CD8\alpha\alpha^{+}$ fate within the IEL[30, 39]. The $CD8\alpha\alpha^{+}CD4^{+}$ T cells show some features of $CD8^{+}$ T_{RM} cells, such as confinement to the epithelial compartment and expression of

canonical tissue residency markers, including CD103, CD244 and granzyme B[30, 39]. The development of these CD8αα $CD4^+$ IEL cells may in part utilise the mechanistic underpinnings described here. In steady-state conditions, it had been shown that ectopic expression of Runx3 in $CD4^+$ T cells induces the expression of CD103 in lymphoid and non-lymphoid tissues without increasing $CD4^+$ T cell frequencies in the small intestine or redirecting them towards the CD8αα lineage[40]. We found that ectopic Runx3 can enhance intra-epithelial $CD4^+$ T_{RM} cell numbers and decrease tissue exit after virus infection without inducing CD8α expression. Combined, these results argue that CD103 expression and intraepithelial localisation are stand-alone features driven by Runx3, suggesting that complete CD8αα lineage conversion may have additional requirements.

While $CD8^+$ T_{RM} cells largely remain in their original tissue of lodgement[41], antigen restimulation can promote some level of egress, with ex-T_{RM} cells capable of populating lymphoid organs and contributing to circulating immunity[42, 43]. Partial recirculation is also seen in the liver in $CD103^-CD8^+$ T_{RM} cells that have not undergone complete TGFβ-mediated maturation[9]. Thus, tissue exit, whether by $CD4^+$ or $CD8^+$ T_{RM} cells, could reflect a lack of full engagement of the TGFβ-mediated residency program, which results in a transient form of tissue residency, with concomitant retention of memory cell plasticity. Consistent with this, human $CD4^+$ T_{RM}-like cells can continuously migrate between skin and blood[44]. Parabiosis experiments in mice also showed some level of recirculation of skin $CD4^+$ T_{RM} cells[19]. Teleologically, a less stringent form of retention for $CD4^+$ T cells may relate to their prolonged ability to enter peripheral tissues[13, 19], unlike $CD8^+$ T_{RM} cells, which lose this capability soon after antigen stimulation[21, 45].

Understanding the factors involved in T_{RM} cell development and functionality is crucial to manipulate these cells for therapeutic gain. Of note, we observed an increased ability of CD4-Runx3 cells to control local infection. In line with this, $CD4^+$ T cell populations with increased Runx3 expression and cytotoxic features have been associated with pathogen and tumour control in various patient cohorts[46, 47]. While such elevated effector-type functionality has obvious benefits in diseases, its potential for autoimmune tissue destruction may be one reason why tissue residency tends to be more transient in the $CD4^+$ T_{RM} cell population[13] or why resident $CD4^+$ T cells are often biased towards regulatory functionality and tissue repair[48, 49].

Finally, it remains unclear whether Runx3 underpins other differences between the $CD4^+$ and $CD8^+$ T_{RM} cell subsets, such as requirements for antigen stimulation or cytokines that extend beyond TGFβ[19, 20]. Overall, our study showed that $CD4^+$ and $CD8^+$ T_{RM} cells were not equivalent in the context of tissue residency. Instead, the central role of Runx3 in $CD8^+$ T_{RM} cell development and its natural attenuation in the $CD4^+$ T_{RM} cell subset results in unique forms of tissue residency that shapes the persistence, distribution, migration and function of these unique cell types.

Acknowledgements. We thank the Flow Cytometry Unit and Bioresources Facility at Peter Doherty Institute (University of Melbourne) for technical assistance. This work was supported by a Howard Hughes Medical Institute and Bill & Melinda Gates International Research Scholarship OPP1175796, National Health and Medical Research Council (NHMRC) AP1113293 to F.RC. and L.K.M. S.L.P. was supported by a NHMRC EL1 Investigator Grant GNT1175626. N.G.Z. was supported by FAPESP (BEPE 2019/12431-2). A.T.S. was supported by the National Institutes of Health (U01CA260852 and UM1HG012076), the Parker Institute for Cancer Immunotherapy, and a Pew-Stewart Scholars for Cancer Research Award. L.K.M is a Senior Medical Research Fellow supported by the Sylvia and Charles Viertel Charitable Foundation. The authors declare no competing financial interests.

Author contributions. R.F., T.N.B., L.C.G., S.D., A.O., S.L.P., M.E., S.K.S., S.N.C., N.M.Z., N.G.Z., F.A.B., C.L., K.M., and A.Z. performed experiments and analysed data; S.N.M., T.P.S., A.S. and L.K.M. provided supervision; R.F., T.N.B., S.L.P., F.R.C. and L.K.M. contributed to experimental design; R.F., T.N.B., F.R.C. and L.K.M. prepared the manuscript; A.S., F.R.C. and L.K.M. provided funding; L.K.M. and F.R.C. led the research program.

Competing interests. The authors declare no competing interests. A.T.S. is a founder of Immunai and Cartography Biosciences and receives unrelated research funding from Merck Research Laboratories, Allogene Therapeutics, and Arsenal Biosciences.

Figure Legends

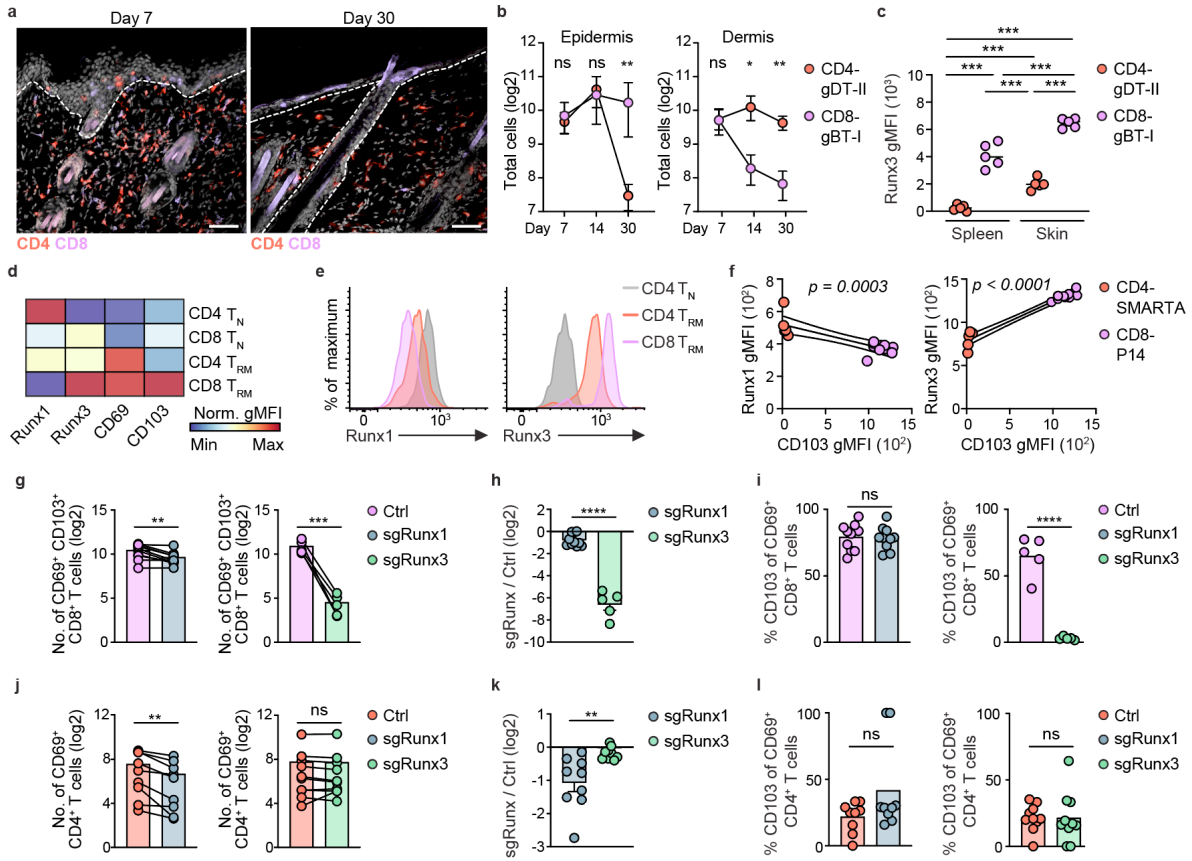

Figure 1. Runx1 and Runx3 differentially program CD4$^+$ and CD8$^+$ T$_{RM}$ cell development. (a) Microscopy showing CD4$^+$ and CD8$^+$ T cells in skin 7 or 30 days post-HSV infection (d.p.i.). Scale bar=50µm. **(b)** Kinetics of CD4$^+$ gDT-II and CD8$^+$ gBT-I cells in epidermis (***P*=0.0079) and dermis (**P*=0.0317, ***P*=0.0079, two-tailed Mann-Whitney's test) at 7, 14 and 30 d.p.i. **(c)** Runx3 expression in spleen and skin 30d post-HSV infection. (****adjP* <0.001, ANOVA with Tukey's multiple comparisons test). **(d-f)** Expression of Runx1, Runx3, CD69, and CD103 in naïve (CD44$^-$CD62L$^+$, spleen), CD69$^+$CD4$^+$ SMARTA (SI-LP) and CD69$^+$CD103$^+$CD8$^+$ P14 (SI-IEL) T$_{RM}$ cells at >30 d.p.i. with LCMV via heatmap **(d)**, histograms **(e)**, correlation plots of Runx1 or Runx3 vs. CD103 (linear regression line, 95% confidence interval, *P* showing slope is non-zero) **(f)**. **(g-i)** Enumeration of CD8$^+$ T$_{RM}$ cells (***P*=0.0015,****P*=0.0002, two-tailed paired t-test) **(g)**, log2-fold change (*****P*=0.0007, unpaired t-test) **(h)**, and CD103 expression in CD69$^+$CD8$^+$ cells (*****P*=0.0007, paired t-test) **(i)**, in CRISPR-Cas9 ablated Ctrl, sgRunx1, and sgRunx3 gBT-I cells in skin >20d post-i.d. transfer. **(j-l)** As for (g-i) but in gDT-II cells (***P*=0.0040, two-tailed paired; ***P*=0.0010, unpaired t-test respectively). **(a-c)** Data representative of 2 independent experiments with **(a)** n=4, **(b, c)** n=5 mice. Data pooled from **(d-f)** 2 independent

experiments with n=5 mice containing P14 and SMARTA and n=5 containing P14, **(g-i)** n=5, **(j-l)** n=4 and n=5 or 1 experiment for CD8$^+$ sgRunx3. Symbols represent **(b)** mean, **(c, f-l)** mice, bars mean, error bars indicate SEM.

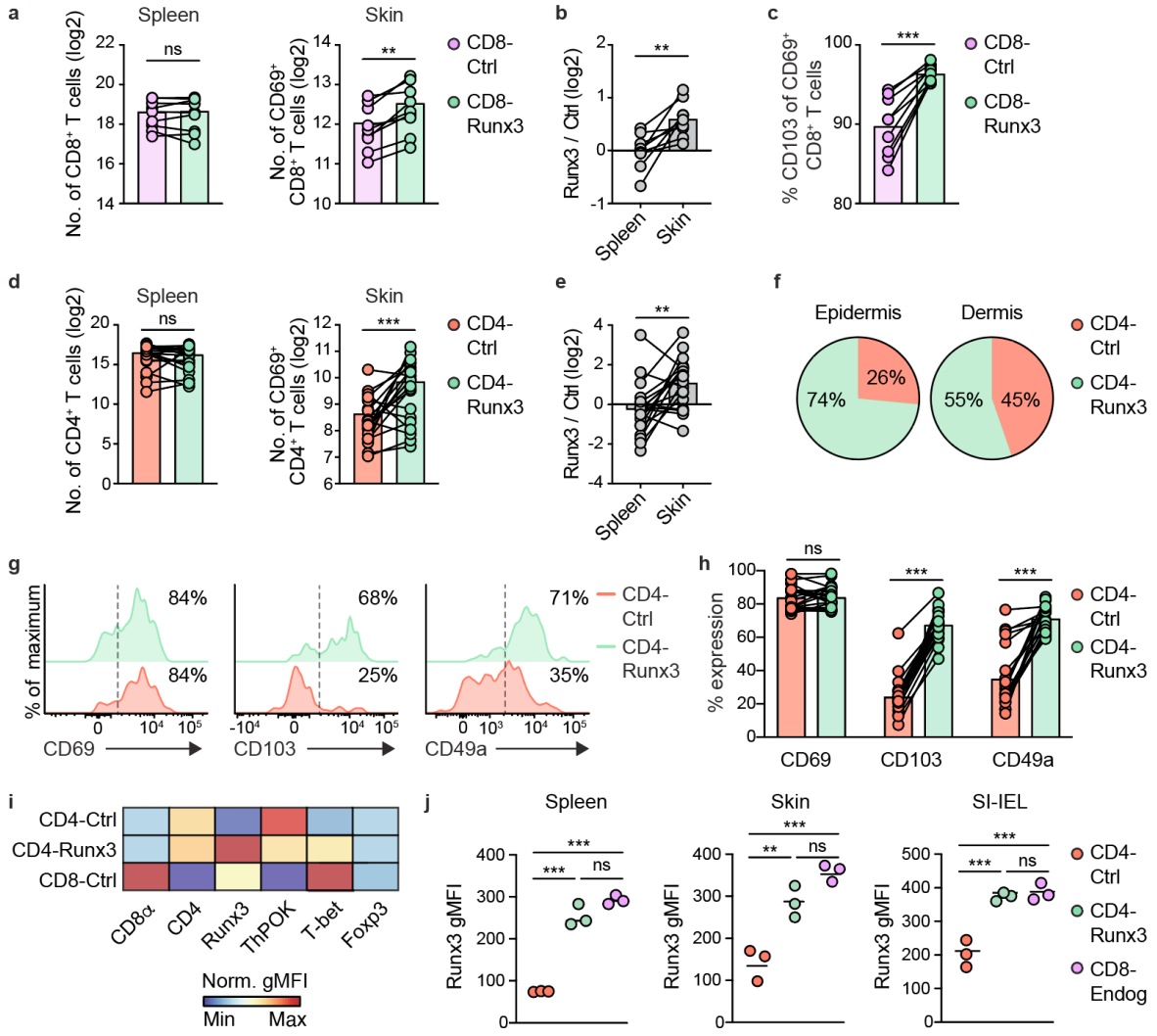

Figure 2. Enforced Runx3 expression increases epithelial residency in CD4$^+$ T cells. (a-c) Enumeration of CD8$^+$ gBT-I cells transduced with control (CD8-Ctrl) or Runx3-expressing (CD8-Runx3) retroviruses in spleen and skin (***P*=0.0073, two-tailed paired t-test) **(a)**, log2-fold change (***P*=0.0036, paired t-test) **(b)**, and CD103 expression in skin (****P*=0.0001, paired t-test) **(c)** at 14 d.p.i. with HSV. **(d-h)** Enumeration of CD4$^+$ gDT-II cells transduced with control (CD4-Ctrl) or Runx3-expressing (CD4-Runx3) retroviruses in spleen and skin (****P*=0.0010, two-tailed paired t-test) **(d)**, log2-fold change (***P*=0.0026, paired t-test) **(e)**, proportion of cells in the epidermis and dermis **(f)**, representative histograms **(g)** and percent expression of CD69, CD103 and CD49a (****adjP*<0.0001, multiple paired t-tests) in skin **(h)** at 14 d.p.i. with HSV. **(i)** Heatmap showing expression of CD8α, CD4, Runx3, ThPOK, T-bet

and Foxp3 by transduced cells as in (a-h) *in vitro* before transfer. **(j)** Runx3 expression by gDT-II transduced cells as in (d-h) at 14 d.p.i. (spleen and skin) or SMARTA (SI-IEL) cells and endogenous CD8$^+$ T cells after HSV or LCMV infection respectively (**$adjP$=0.07, ***$adjP$<0.001, ANOVA with Tukey's multiple comparisons test). **(a-h)** Data pooled from 2 independent experiments with **(a-c)** n=5, and n=4 or **(d-h)** n=10 mice. **(i,j)** Data representative of 2 independent experiments, with n=3 mice. Bars indicate mean, dots indicate individual mice.

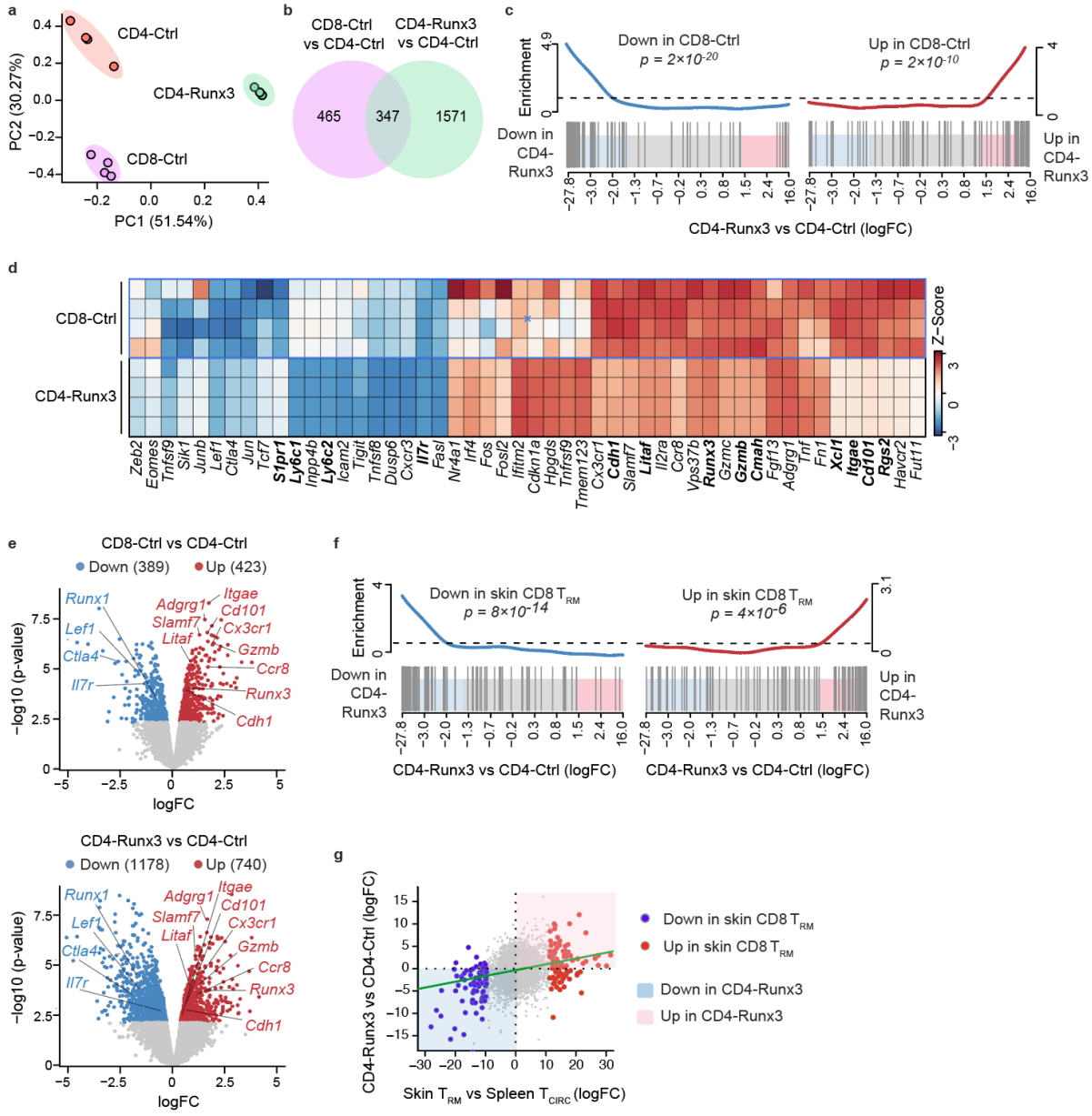

Figure 3. Runx3 induces a CD8-like T_{RM} cell transcriptional signature in CD4$^+$ T cells.
(a) PCA of gene expression differences between control retrovirus transduced gBT-I cells (CD8-Ctrl), control retrovirus transduced gDT-II cells (CD4-Ctrl), or Runx3 retrovirus

transduced gDT-II cells (CD4-Runx) isolated from the skin 14d post-HSV infection. **(b)** Venn diagram showing differences in gene expression between CD8-Ctrl vs CD4-Ctrl, and CD4-Runx3 vs CD4-Ctrl cells. **(c)** Barcode plots of the CD4-Runx3 gene signature in top ranked CD8-Ctrl genes (standardised log2-fold change). **(d)** Heatmap showing DEGs in CD8-Ctrl and CD4-Runx3 cells relative to CD4-Ctrl (rows represents independent samples, color scale based on Z-score distribution). **(e)** Volcano plots of DEGs between CD8-Ctrl and CD4-Ctrl or CD4-Runx3 and CD4-Ctrl (gray dots represent genes not DE). **(f)** Barcode plots of the CD4-Runx3 gene signature for top ranked skin T_{RM} vs splenic T_{CIRC} cells genes from GSE70813 (standardised log2-fold change). **(g)** Scatter plot showing transcriptional changes for skin T_{RM} vs splenic T_{CIRC} and CD4-Runx3 vs CD4-Ctrl for all genes (dots represent DEG in Skin T_{RM} vs Splenic T_{CIRC}, shaded quadrants represent DEG in CD4-Runx3 vs CD4-Ctrl). Data pooled from 2 independent experiments, n=2 biological replicates pooled from 10 mice. Green line represents least-squares regression line.

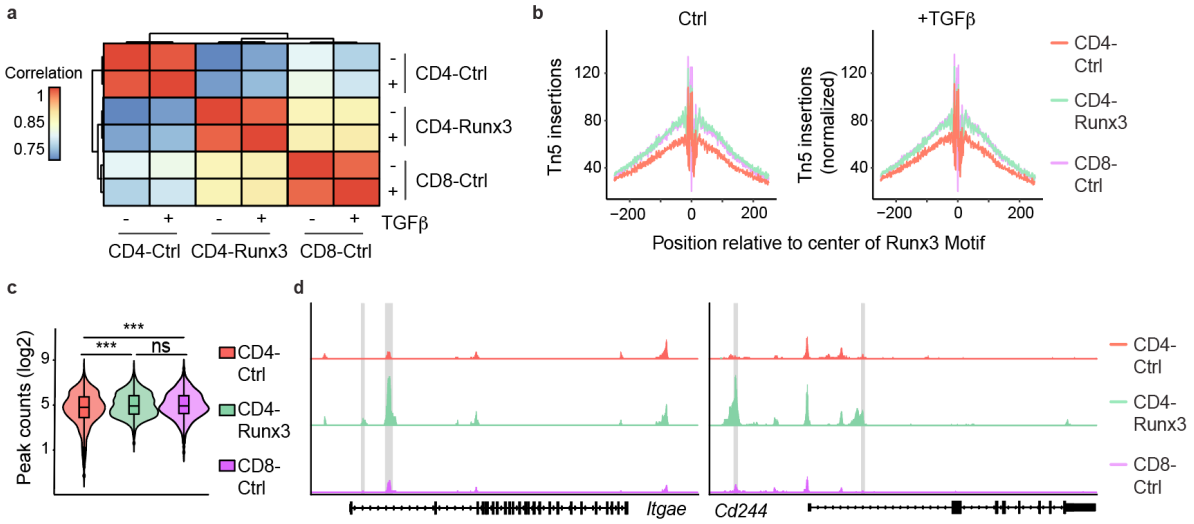

Figure 4. Runx3 promotes chromatin accessibility at TGFβ regulated genes. (a-d) Chromatin accessibility correlation matrix **(a)**, Runx3 footprint (normalised) in control or TGFβ treated cells **(b)**, number of peaks in regions associated with TGFβ-induced genes from GSE178769 (***$P \leq 0.001$, Wilcoxon test) **(c)** and *Itgae* and *Cd244* genome tracks (height normalised) **(d)** in $CD8^+$ gBT-I cells transduced with control (CD8-Ctrl), $CD4^+$ gDT-II cells transduced with control (CD4-Ctrl), or $CD4^+$ gDT-II cells transduced with Runx3-expressing (CD4-Runx3) retroviruses cultured +/- TGFβ for 48 hours. Data representative of 2 independent experiments, with n=2 technical replicates. Violin plots represent distribution of minimum-maximum values, line represents median, boxes indicate interquartile range.

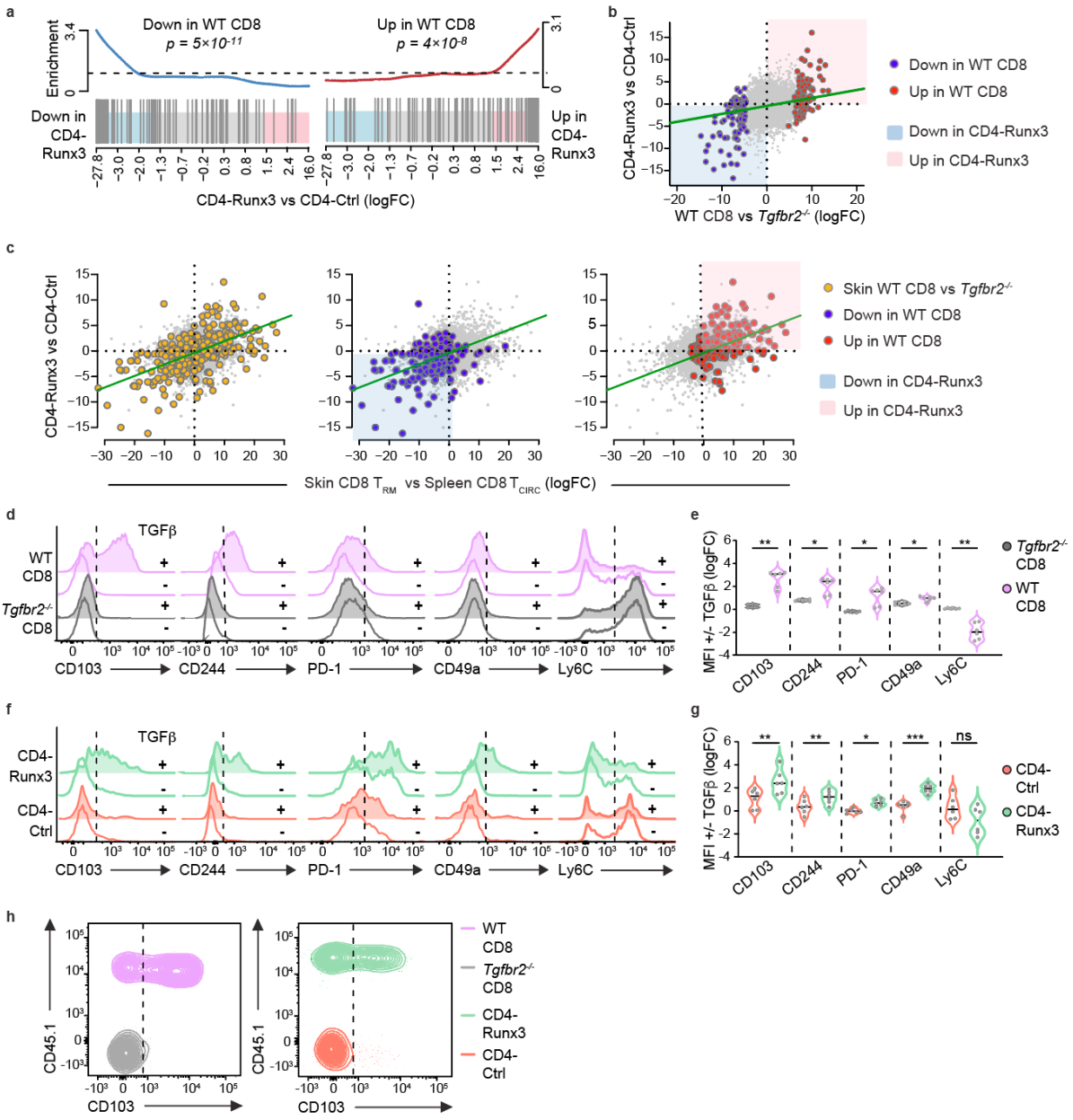

Figure 5. Runx3 programs TGFβ-responsiveness in CD4$^+$ T cells to establish a CD8$^+$ T$_{RM}$ cell-like transcriptome in skin. (a-c) Barcode plots of CD4-Runx3 gene signature in the top ranked TGFβ-regulated DEGs from GSE178769 **(a)**, scatter plot showing transcriptional changes for skin WT CD8$^+$ vs *Tgfbr2*$^{-/-}$ CD8$^+$ cells and CD4-Runx3 vs CD4-Ctrl for all genes **(b)**, scatter plots of skin T$_{RM}$ vs splenic T$_{CIRC}$ and CD4-Runx3 vs CD4-Ctrl log-fold changes (orange dots denote TGFβ-regulated genes in skin WT CD8, blue and red dots show top 200 down- or up-regulated genes in skin WT CD8) **(c)** in transduced cells (as in Fig. 3). **(d, e)** Representative histograms **(d)** and violin plots showing log2-fold change in CD103, CD244, PD-1, CD49a and Ly6C expression (MFI) (*adjP*=0.002, 0.043, 0.039, 0.028, 0.006 respectively, ANOVA with Bonferroni's multiple comparisons test) **(e)** in control transduced wild-type OT-I (WT CD8) and *Tgfbr2*$^{-/-}$ (*Tgfbr2*$^{-/-}$CD8) cells cultured +/- TGFβ for 48 hours.

(f, g) As in (d, e) but with gDT-II cells transduced with control (CD4-Ctrl) or Runx3-expressing (CD4-Runx3) retroviruses (*adjP*=0.008, 0.010, 0.024, <0.001, 0.403, ANOVA with Bonferroni's multiple comparisons test). **(h)** CD103 expression in WT CD8, *Tgfbr2*$^{-/-}$ CD8, CD4-Ctrl and CD4-Runx3 cells. Data pooled from **(a-c)** 2 independent experiments, n=2 biological replicates pooled from 10 mice or **(d-h)** 3 independent experiments, n=2 biological replicates. **(e, g)** Symbols represent biological replicates. **(b-c)** Green line represents least-squares regression line. Violin plots represent distribution of minimum-maximum values, line indicates median.

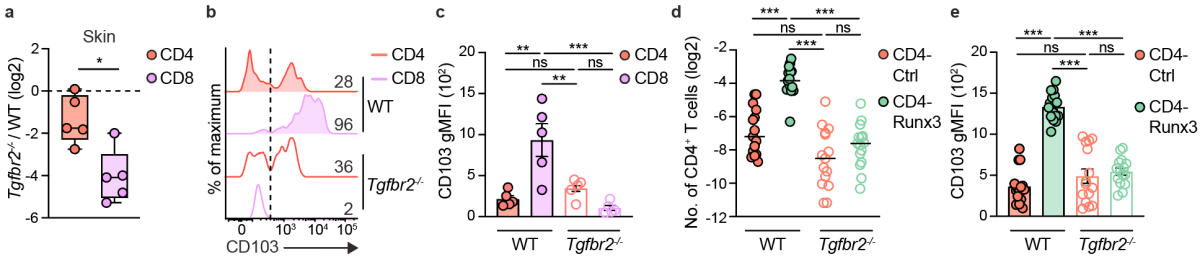

Figure 6. Runx3-induced tissue residency depends on TGFβ signalling. (a-c) Log2-fold change of WT and *Tgfbr2*$^{-/-}$ CD69^{+} CD4^{+} and CD8^{+} T cells in skin normalised to spleen (**P*=0.0288, paired t-test) **(a)**, representative histograms **(b)** and CD103 expression (gMFI, ***adjP*=0.001 and 0.005, ****adjP*<0.001, ANOVA with Tukey's multiple comparisons test) **(c)** in WT and *Tgfbr2*$^{-/-}$ CD4^{+} and CD8^{+} T cells isolated from skin 30d post-i.d. transfer. **(d, e)** Enumeration of Ctrl- and Runx3-transduced WT and *Tgfbr2*$^{-/-}$ CD69^{+} CD4^{+} T cells in skin normalised to spleen (****adjP*<0.001, ANOVA with Tukey's multiple comparisons test) **(d)**, and CD103 expression (gMFI, ****adjP*<0.001, ANOVA with Tukey's multiple comparisons test) **(e)** in WT and *Tgfbr2*$^{-/-}$ CD4^{+} T cells transduced with control (WT Ctrl and *Tgfbr2*$^{-/-}$ Ctrl) or Runx3-expressing (WT Runx3 and *Tgfbr2*$^{-/-}$ Runx3) retroviruses isolated from skin 14d post-i.d. transfer. Data representative of **(a-c)** 2 independent experiments, n=5 or pooled from **(d, e)** 3 independent experiments, n=5 mice. Symbols represent mice, bars indicate mean, error bars indicate SEM. Box plots show the median, interquartile range, and minimum/maximum whiskers.

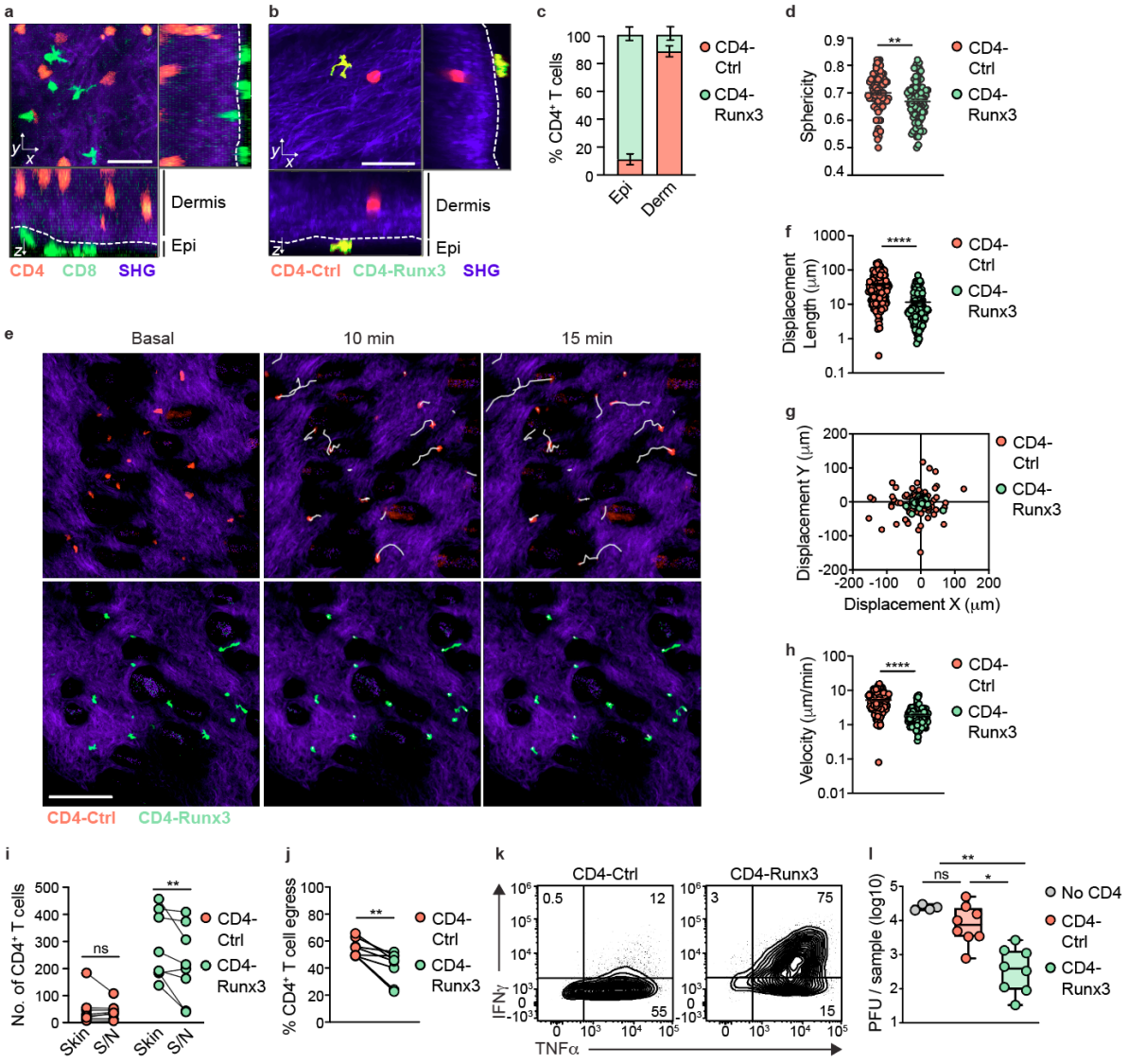

Figure 7. Runx3 enforces protective CD8$^+$ T$_{RM}$ cell-like immune surveillance by CD4$^+$ T cells in skin. (a) Maximum intensity projection with CD4$^+$ gDT-II and CD8$^+$ gBT-I cells in skin 20d post-HSV infection. Second harmonic generation (SHG). **(b-h)** Maximum intensity projections **(b)**, epidermis/dermis proportion **(c)**, sphericity (***P*=0.0055, two-tailed unpaired t-test) **(d),** migration tracks **(e)**, track displacement length (*****P*<0.0001) **(f)**, displacement **(g)**, and velocity (*****P*<0.0001) **(h)** in CD4$^+$ ubiTomato and GFP T cells transduced with control (CD4-Ctrl) or Runx3 (CD4-Runx3) retroviruses in skin 14d post-i.d. transfer. **(i, j)** Enumeration of Ctrl- and Runx3-transduced cells in supernatant (S/N) or skin (***P*=0.0317, multiple paired t-tests) **(i)** and proportion of egressing cells (***P*=0.051, two-tailed paired t-test) **(j)** from skin explants with gDT-II cells transduced with control (CD4-Ctrl) or Runx3 (CD4-Runx3) retroviruses cultured overnight. **(k)** Representative plots showing IFNγ and TNFα production by CD4-Ctrl or CD4-Runx3 cells 4 hours after PMA/Ionomycin. **(l)** Viral titre in skin of *Rag1*$^{-/-}$ mice transferred i.d. with CD4-Ctrl or CD4-Runx3 cells 6 d.p.i.

(*$adjP$=0.0181, **$adjP$=0.031, Kruskal-Wallis with Dunn's test). Data representative of 2 independent experiments with **(a)** n=3 or pooled from 2 independent experiments with **(b-h)** n=4 and 5 (Ctrl) and n=4 (Runx3), **(i, j)** n=8 mice, **(k)** n=2 biological replicates, **(l)** n=4 mice (or n=2 for no-CD4). Symbols represent **(d, f-h)** cells or **(i, j, l)** mice, bars indicate mean, error bars indicate SEM. Box plots show median, interquartile range, minimum/maximum whiskers. Scale bars=30 **(a, b)** or 100μm **(e)**.

References

1. Jameson, S.C. & Masopust, D. Understanding Subset Diversity in T Cell Memory. *Immunity* **48**, 214-226 (2018).

2. Masopust, D. & Soerens, A.G. Tissue-Resident T Cells and Other Resident Leukocytes. *Annual Review of Immunology* **37**, 521-546 (2019).

3. Mackay, L.K. *et al.* The developmental pathway for CD103+CD8+ tissue-resident memory T cells of skin. *Nature Immunology* **14**, 1294-1301 (2013).

4. Kok, L. *et al.* A committed tissue-resident memory T cell precursor within the circulating CD8+ effector T cell pool. *Journal of Experimental Medicine* **217** (2020).

5. Kurd, N.S. *et al.* Early precursors and molecular determinants of tissue resident memory CD8+ T lymphocytes revealed by single-cell RNA sequencing. *Science Immunology* **5** (2020).

6. Kok, L., Masopust, D. & Schumacher, T.N. The precursors of CD8+ tissue resident memory T cells: from lymphoid organs to infected tissues. *Nature Reviews Immunology* (2021).

7. Hirai, T. *et al.* Keratinocyte-Mediated Activation of the Cytokine TGF-β Maintains Skin Recirculating Memory CD8+ T Cells. *Immunity* **50**, 1249-1261.e1245 (2019).

8. Zhang, N. & Bevan, J.M. Transforming Growth Factor-β Signaling Controls the Formation and Maintenance of Gut-Resident Memory T Cells by Regulating Migration and Retention. *Immunity* **39**, 687-696 (2013).

9. Christo, S.N. *et al.* Discrete tissue microenvironments instruct diversity in resident memory T cell function and plasticity. *Nature Immunology* (2021).

10. Skon, C.N. *et al.* Transcriptional downregulation of S1pr1 is required for the establishment of resident memory CD8+ T cells. *Nature Immunology* **14**, 1285-1293 (2013).

11. Mackay, L.K. *et al.* Hobit and Blimp1 instruct a universal transcriptional program of tissue residency in lymphocytes. *Science* **352**, 459-463 (2016).

12. Milner, J.J. *et al.* Runx3 programs CD8+ T cell residency in non-lymphoid tissues and tumours. *Nature* **552**, 253-257 (2017).

13. Beura, L.K. *et al.* CD4+ resident memory T cells dominate immunosurveillance and orchestrate local recall responses. *Journal of Experimental Medicine* **216**, 1214-1229 (2019).

14. Nguyen, Q.P., Deng, T.Z., Witherden, D.A. & Goldrath, A.W. Origins of CD 4 + circulating and tissue-resident memory T-cells. *Immunology* **157**, 3-12 (2019).

15. Schreiner, D. & King, C.G. CD4+ Memory T Cells at Home in the Tissue: Mechanisms for Health and Disease. *Front Immunol* **9**, 2394 (2018).

16. Hondowicz, B.D., Kim, K.S., Ruterbusch, M.J., Keitany, G.J. & Pepper, M. IL-2 is required for the generation of viral-specific CD4+ Th1 tissue-resident memory cells and B cells are essential for maintenance in the lung. *European Journal of Immunology* **48**, 80-86 (2018).

17. Turner, D.L. & Farber, D.L. Mucosal resident memory CD4 T cells in protection and immunopathology. *Front Immunol* **5**, 331 (2014).

18. Kumar, B.V. *et al.* Human Tissue-Resident Memory T Cells Are Defined by Core Transcriptional and Functional Signatures in Lymphoid and Mucosal Sites. *Cell Reports* **20**, 2921-2934 (2017).

19. Collins, N. *et al.* Skin CD4+ memory T cells exhibit combined cluster-mediated retention and equilibration with the circulation. *Nature Communications* **7**, 11514 (2016).

20. Iijima, N. & Iwasaki, A. A local macrophage chemokine network sustains protective tissue-resident memory CD4 T cells. *Science* **346**, 93-98 (2014).

21. Gebhardt, T. *et al.* Different patterns of peripheral migration by memory CD4+ and CD8+ T cells. *Nature* **477**, 216-219 (2011).

22. Ariotti, S. *et al.* Tissue-resident memory CD8+ T cells continuously patrol skin epithelia to quickly recognize local antigen. *Proceedings of the National Academy of Sciences* **109**, 19739-19744 (2012).

23. Steinert, E.M. *et al.* Quantifying Memory CD8 T Cells Reveals Regionalization of Immunosurveillance. *Cell* **161**, 737-749 (2015).

24. Shin, B. *et al.* Runx1 and Runx3 drive progenitor to T-lineage transcriptome conversion in mouse T cell commitment via dynamic genomic site switching. *Proc Natl Acad Sci U S A* **118** (2021).

25. Setoguchi, R. *et al.* Repression of the Transcription Factor Th-POK by Runx Complexes in Cytotoxic T Cell Development. *Science* **319**, 822-825 (2008).

26. Luckey, M.A. *et al.* The transcription factor ThPOK suppresses Runx3 and imposes CD4+ lineage fate by inducing the SOCS suppressors of cytokine signaling. *Nature Immunology* **15**, 638-645 (2014).

27. Ciucci, T. *et al.* The Emergence and Functional Fitness of Memory CD4+ T Cells Require the Transcription Factor Thpok. *Immunity* **50**, 91-105.e104 (2019).

28. Djuretic, I.M. *et al.* Transcription factors T-bet and Runx3 cooperate to activate Ifng and silence Il4 in T helper type 1 cells. *Nature Immunology* **8**, 145-153 (2007).

29. Komine, O. *et al.* The Runx1 Transcription Factor Inhibits the Differentiation of Naive CD4+ T Cells into the Th2 Lineage by Repressing GATA3 Expression. *Journal of Experimental Medicine* **198**, 51-61 (2003).

30. Reis, B.S., Rogoz, A., Costa-Pinto, F.A., Taniuchi, I. & Mucida, D. Mutual expression of the transcription factors Runx3 and ThPOK regulates intestinal CD4+ T cell immunity. *Nature Immunology* **14**, 271-280 (2013).

31. Mackay, L.K. *et al.* Hobit and Blimp1 instruct a universal transcriptional program of tissue residency in lymphocytes. *Science* **352**, 459-463 (2016).

32. Mackay, L. *et al.* T-box Transcription Factors Combine with the Cytokines TGF-β and IL-15 to Control Tissue-Resident Memory T Cell Fate. *Immunity* **43**, 1101-1111 (2015).

33. Wang, D. *et al.* The Transcription Factor Runx3 Establishes Chromatin Accessibility of cis-Regulatory Landscapes that Drive Memory Cytotoxic T Lymphocyte Formation. *Immunity* **48**, 659-674.e656 (2018).

34. Schenkel, J.M. *et al.* T cell memory. Resident memory CD8 T cells trigger protective innate and adaptive immune responses. *Science* **346**, 98-101 (2014).

35. Ariotti, S. *et al.* T cell memory. Skin-resident memory CD8(+) T cells trigger a state of tissue-wide pathogen alert. *Science* **346**, 101-105 (2014).

36. Taniuchi, I. *et al.* Differential Requirements for Runx Proteins in CD4 Repression and Epigenetic Silencing during T Lymphocyte Development. *Cell* **111**, 621-633 (2002).

37. Moreau, J.M., Velegraki, M., Bolyard, C., Rosenblum, M.D. & Li, Z. Transforming growth factor-beta1 in regulatory T cell biology. *Sci Immunol* **7**, eabi4613 (2022).

38. Korn, T., Bettelli, E., Oukka, M. & Kuchroo, V.K. IL-17 and Th17 Cells. *Annu Rev Immunol* **27**, 485-517 (2009).

39. Mucida, D. *et al.* Transcriptional reprogramming of mature CD4+ helper T cells generates distinct MHC class II–restricted cytotoxic T lymphocytes. *Nature Immunology* **14**, 281-289 (2013).

40. Keller, H.R. *et al.* The molecular basis and cellular effects of distinct CD103 expression on CD4 and CD8 T cells. *Cellular and Molecular Life Sciences* **78**, 5789-5805 (2021).

41. Gebhardt, T. *et al.* Memory T cells in nonlymphoid tissue that provide enhanced local immunity during infection with herpes simplex virus. *Nature Immunology* **10**, 524-530 (2009).

42. Fonseca, R. *et al.* Developmental plasticity allows outside-in immune responses by resident memory T cells. *Nature Immunology* **21**, 412-421 (2020).

43. Stolley, J.M. *et al.* Retrograde migration supplies resident memory T cells to lung-draining LN after influenza infection. *Journal of Experimental Medicine* **217** (2020).

44. Klicznik, M.M. *et al.* Human CD4+CD103+ cutaneous resident memory T cells are found in the circulation of healthy individuals. *Science Immunology* **4**, eaav8995 (2019).

45. Masopust, D. *et al.* Dynamic T cell migration program provides resident memory within intestinal epithelium. *Journal of Experimental Medicine* **207**, 553-564 (2010).

46. Oh, D.Y. & Fong, L. Cytotoxic CD4(+) T cells in cancer: Expanding the immune effector toolbox. *Immunity* **54**, 2701-2711 (2021).

47. Cheroutre, H. & Husain, M.M. CD4 CTL: Living up to the challenge. *Seminars in Immunology* **25**, 273-281 (2013).

48. Delacher, M. *et al.* Single-cell chromatin accessibility landscape identifies tissue repair program in human regulatory T cells. *Immunity* **54**, 702-720 e717 (2021).

49. Durand, A. *et al.* Profiling the lymphoid-resident T cell pool reveals modulation by age and microbiota. *Nature Communications* **9** (2018).

50. Zaid, A. *et al.* Persistence of skin-resident memory T cells within an epidermal niche. *Proceedings of the National Academy of Sciences* **111**, 5307-5312 (2014).

Methods

Mice. C57BL/6, B6.SJL-PtprcaPep3b/BoyJ (CD45.1), C57BL/6 × B6.SJL-PtprcaPep3b/BoyJ (CD45.1.2), ubiTomato, uGFP, gBT-I:CD45.1, gBT-I:CD45.1.2, gDT-II:CD45.1.1, gDT-II:CD45.1.2, gDT-II:CD45.2, SMARTA:uGFP, SMARTA:Thy1.1, SMARTA:Thy1.1.CD45.1, P14:CD45.1, P14:Thy1.1, Tgfbr2$^{flox/flox}$.dLck-cre:CD45.1 (*Tgfbr2*$^{-/-}$), *Rag1*$^{-/-}$ (B6.129S7.Rag1tm/mom/J) female mice were bred and maintained in the Department of Microbiology and Immunology, University of Melbourne under a 12/12 hour light/dark cycle, at 19-22^{o}C and 40-70% humidity. All experiments were approved by the University of Melbourne Animal Ethics Committee (ID #21651 and #1714105). All mice were used between 6 and 20 weeks of age.

Adoptive cell transfers, infections and DNFB treatment. For naïve transgenic T cell transfers, cells were isolated from lymph nodes and transferred intravenously (i.v). CD8^{+} T cells were transferred at 5×10^{4} cells and CD4^{+} T cells at 1×10^{4} cells per recipient. Transduced cells were mixed at a 1:1 ratio and 2.5×10^{5} cells were transferred i.v. or 1×10^{6} cells were transferred intradermally (i.d.) into recipient mice. Skin infections were performed by skin scarification with 1×10^{6} plaque-forming units (PFU) of HSV-1 KOS or HSV KOS.CreTK^{-} as described[41]. Mice were shaved and depilated before treatment with 15 µl of DNFB (Sigma-Aldrich) diluted at 0.25% in acetone:oil (4:1) on the skin. LCMV Armstrong infections were done by intraperitoneal injection of 2×10^{5} PFU.

Retroviral transduction. For transfections, 293T cells were seeded into 96-mm dishes at a density of 5×10^{6} cells the day before transfection. Cells were transfected with empty- or Runx3-MigR1-GFP based retroviral vectors kindly provided by A. Goldrath (University of California, UCSD), and pCL-Eco (Addgene #12371) using the CalPhos Mammalian Transfection Kit (Takara). Viral supernatant was harvested after 48 hours, filtered (0.45 µm; Millipore), and 0.5 ml was spun down onto 24-well plates pre-coated with RetroNectin (20 µg/ml; Takara). Naïve CD4^{+} T cells were negatively enriched from spleen and lymph nodes of naïve ubiTomato, uGFP, gDT-II and SMARTA mice by incubating cell suspension with anti-CD8, anti-CD11b anti-F4/80, anti-Ter119 and anti-I-A/I-E monoclonal antibodies. Naïve CD4^{+} T cells were further positively enriched using magnetically labelled anti-CD4 antibodies (Dynabeads mouse CD4, L4T4) and the DetachABead reagent for mouse CD4 (both from Invitrogen Dynal As). Naïve CD8^{+} T cells were negatively enriched from spleen and lymph

nodes of gBT-I and P14 mice by incubating cell suspension with anti-CD4, anti-CD11b anti-F4/80, anti-Ter119 and anti-I-A/I-E monoclonal antibodies, followed by incubation with goat anti-rat IgG-coupled magnetic beads (Qiagen) before removing bead-bound cells. Enriched cells were plated in 24-well plates (Thermo Fisher Scientific) precoated with anti-CD3 (clone 144-2C11) and anti-CD28 (37.51) (5 μg/ml; eBioscience) at 1×10^6 cells/well for 24 hours ($CD8^+$ T cells) or 48 hours ($CD4^+$ T cells). *In vitro* activated cells were transferred to 24-well plates containing viral supernatant and expanded for 3 days in the presence of recombinant human interleukin-2 (IL-2, 25 U/ml; PeproTech) at 37ºC, 5%CO_2.

CRISPR/Cas9 gene editing of $CD8^+$ T cells. Single guide RNAs (sgRNA) targeting: *Runx1* (5'-CCUGGCCUGGGUUGCACGU-3', 5'-GAGAAGCUGGCUUGGUAUCG-3'), *Runx3* (5'-AGACAGGTACTGAGACTCGGCGG-3', 5'-GTTGACCCTTATGACATGCCAGG-3'), and *Cd19* (5'-AAUGUCUCAGACCAUAUGGG-3') were purchased from Synthego (CRISPRevolution sgRNA EZ Kit). sgRNA/Cas9 RNPs were formed by incubating 0.3nmol of sgRNA with 0.6 μl Alt-R S.p. Cas9 nuclease V3 (10 mg/ml; Integrated DNA Technologies) for 10 min at room temperature. Naïve gBT-I and gDT-II cells were enriched as for transduction, then $1x10^7$ T cells were resuspended in 20μl of P3 (P3 Primary Cell 4D-Nucleofector X Kit; Lonza), mixed with sgRNA/Cas9 RNP and electroporated using a Lonza 4D-Nucleofector system (DN100). Cells were rested for 30min in 96well plate prior to activation in culture for 5d with peptide pulsed splenocytes ($gB_{498-505}$ (SSIEFARL) for gBT-I; $gB_{315-327}$ (IPPNWHIPSIQDA) for gDT-II) in the presence of IL-2 (25 U/mL, Peprotech) at 37ºC, 5%CO_2, or transferred immediately into mice then infected with LCMV-Armstrong. Control (sgCD19) and Runx-edited (sgRunx1 or sgRunx3) cells were mixed at a 1:1 ratio and 1×10^7 cells were transferred i.d. into the skin of naïve recipients.

Organ processing, flow cytometry, and cell sorting. Spleens were processed through metal meshes into single-cell suspensions followed by red blood cell lysis. Skin samples were excised and incubated at 37°C for 90 min in dispase (2.5 mg/ml; Roche) or liberase (0.25 mg/ml; Sigma) followed by separation of epidermis and dermis. Chopped samples were incubated at 37°C for 30 min in collagenase III (3 mg/ml; Worthington). For isolation of SI-IELs, small intestines were removed, and Peyer's patches were excised. Intestines were cut longitudinally and then laterally in $1cm^2$ pieces. SI pieces were incubated in 10% HBSS/HEPES bicarbonate for 30 min at 37 ºC with 0.154 mg/ml dithioerythritol (DTE). Single cell suspensions were

749 stained with conjugated antibodies for flow cytometry or cell sorting. For intracellular staining
750 of cytokines and transcription factors, cells were pre-fixed with paraformaldehyde (2%;
751 Electron Microscopy Sciences) followed by fixation and permeabilisation using the Foxp3
752 Transcription factor staining buffer set (Invitrogen) as per manufacturer's instructions. The
753 complete list of antibodies, details and dilutions used in this study are listed in Supplementary
754 Table 1. Flow cytometry was performed on a LSRFortessa (BD Biosciences) using FACSDiva
755 v3 or an Aurora (Cytek) using SpectroFlo v3 (Cytek) and analysed with FlowJo software (v9
756 and v10; TreeStar) and Microsoft Excel v16. For cell sorting experiments, transduced gBT-I
757 ($GFP^+CD45.1^+CD45.2^+V\alpha2^+$) and gDT-II ($GFP^+CD45.1^+V\alpha3.2^+$ and $GFP^+CD45.2^+V\alpha3.2^+$)
758 cells were sorted using a FACSAria III (BD Biosciences).
759
760 **Immunofluorescence Staining and Confocal Microscopy.** Skin from the flank of HSV-
761 infected or DNFB-treated mice were fixed in paraformaldehyde buffer, and treated with
762 sucrose for cryopreservation as described[50]. Fixed tissues were embedded in OCT (Tissue Tek
763 IA018; Sakura) and frozen in liquid nitrogen. Tissue sections of 12-25-µm thickness were cut
764 using a cryostat (Leica CM3050S), air-dried and stained with CD4-Alexa Fluor 647 (clone
765 RM4-5) and CD8-Alexa Fluor 488 (clone 53-6.7) antibodies in a semi-humid chamber. Stained
766 sections were incubated with Hoechst nuclear stain (H33258, 1:3000 (vol/vol) in PBS) and
767 mounted with ProLongGold (P36934; Invitrogen). Images were acquired with a LSM780 (Carl
768 Zeiss) microscope using Zen v12 and processed using Imaris v9 (Bitplane), Premiere Pro CS7
769 (Adobe) and ImageJ softwares.
770
771 **Intravital Two-Photon Microscopy.** FACS sorted transduced uGFP and ubiTomato cells
772 were transferred i.d. in the left flank of recipient mice. Mice were anaesthetised with isoflurane
773 (Cenvet; 2.5% for induction, 1.5% for maintenance) vaporised in an 80:20 mixture of oxygen
774 and air using a Tech 3 vaporiser (Surgivet) and injected with 30µL of 0.1% Evans Blue (Sigma-
775 Aldrich) i.v. to visualise blood vessels at least 14 days later. The left flank was shaved and
776 depilated using Veet (Reckitt Benckiser) as described[21]. Two parallel incisions were made
777 through the skin 15 mm apart and the skin was carefully separated from the peritoneum. An
778 18-mm-wide piece of 1-mm stainless steel was inserted under the dermis which was adhered
779 to the steel platform using Vetbond tissue adhesive (3M). Vacuum grease (Dow Corning) was
780 used to attach and seal a glass coverslip onto the epidermis and a moist gauze was placed
781 around the incision to prevent dehydration. Images were acquired with an upright LSM710
782 NLO multiphoton microscope (Carl Zeiss Microimaging) enclosed in a custom-built

783 environmental chamber (Precision Plastics) that was maintained at 35°C with heated air.
784 External nondescanned photomultiplier tube detectors in the reflected light path were used to
785 acquire images. Images were acquired with a 20×/1.0 N.A. water immersion objective.
786 Fluorescence excitation was provided by a Chamelon Vision II Ti:sapphire laser (Coherent),
787 with dispersion correction. uGFP and ubiTomato were excited at 950 nm and at 1100 nm
788 respectively. The collagen-rich dermis of the skin was visualised by second harmonic
789 generation (SHG), using a bandpass 440- to 480-nm filter. Typical voxel dimensions were
790 0.55–0.7 × 0.55–0.7 × 3 μm. For four-dimensional datasets, three dimensional stacks were
791 captured every 1 min for 30–45 min. Raw imaging data were processed with Imaris 7.5
792 (Bitplane). Cell migration was analysed through automatic cell tracking aided by manual
793 corrections. Only tracks that lasted longer than 5 min were analysed. For assessment of cell
794 morphology (sphericity and area), the 3D surface of the cells was rendered in Imaris. Overlay
795 of image sequences and assessment of 2D cell area was calculated using ImageJ. Further edits
796 used Premiere Pro (Adobe).
797
798 ***In vitro*** **stimulation assays.** For TGFβ stimulation, transduced cells were exposed to 10 ng/ml
799 of TGFβ (Peprotech) for 48 hours prior to FACS. To assess cytokine production, transduced
800 cells were incubated with phorbol myristate acetate (PMA; 50ng/ml; Sigma-Aldrich) and
801 Ionomycin (1μg/ml; Sigma-Aldrich) in the presence of Brefeldin A (10μg/ml; Sigma-Aldrich)
802 for 4 hours prior to FACS. Media consisted of complete RPMI (RPMI 1640, 10% FCS, 2mM
803 L-Glutamine, 100 U/ml penicillin, 100 mg/ml streptomycin and 50mM 2-mercaptoethanol).
804
805 ***Ex vivo*** **migration assay.** Skin was excised from HSV-infected mice transferred with
806 transduced T cells. Explants were cultured overnight in complete RPMI 1640. The following
807 day, skin explants were processed as described above and cells that migrated out of the skin
808 were collected from the media. Cells were characterised and counted using flow cytometry.
809
810 **Viral titre determination.** The amount of virus in the skin was determined by PFU assays as
811 described[4]. Briefly, *Rag1*$^{-/-}$ or C57BL/6 mice were transferred with transduced CD4^{+} T cells
812 by i.d. injection and 14 days later infected by skin scarification with 1×10^{6} PFU of HSV
813 KOS.CreTK^{-}. After 6 days, 1cm^{2} of skin was excised and placed in 1 ml of DMEM and frozen
814 for later processing. Samples were homogenised, and 10-fold serial dilutions were tested for
815 plaque formation on confluent Vero cell monolayers to determine viral titre in the original
816 tissue sample.

RNA and ATAC sequencing. For all experimental details and data analysis related to RNA-sequencing and ATAC-sequencing, please refer to the associated Supplementary Information.

Statistical analysis. Statistical analyses were performed using Prism v7 and v9 (GraphPad). Exact *P* values and statistical tests used (two-tailed Mann-Whitney, paired or unpaired t-test, ANOVA with Tukey's or Bonferroni's multiple comparisons test, Kruskal-Wallis with Dunn's test or Wilcoxon test) were indicated in figure legends. $*P < 0.05$; $**P < 0.01$; $***P < 0.001$; $****P < 0.0001$; ns (not significant) $P > 0.05$.

Data availability. All original data is available from the corresponding author upon reasonable request. RNA-seq and ATAC-seq data is available in the Gene Expression Omnibus database under accession codes GSE182511 and GSE198611 respectively. Source Data are provided in the online version of the manuscript.

Code availability. The code generated and used for the analysis of sequencing data are available from the corresponding author on reasonable request.

Additional information. Supplementary information is available for this paper.
Correspondence and request for materials should be addressed to L.K.M. Reprints and permission information is available at www.nature.com/reprints.